J|A|C|S
ARTICLES
Published on Web 10/18/2005

Direct Observation of a Transverse Vibrational Mechanism for Negative Thermal Expansion in $Zn(CN)_2$: An Atomic Pair Distribution Function Analysis

Karena W. Chapman,[†] Peter J. Chupas,[‡] and Cameron J. Kepert*,[†]

Contribution from the School of Chemistry, University of Sydney, Sydney, NSW 2006 Australia; Advanced Photon Source, Argonne National Laboratory, Argonne, Illinois 60439

Received July 31, 2005; E-mail: c.kepert@chem.usyd.edu.au

Abstract: The instantaneous structure of the cyanide-bridged negative thermal expansion (NTE) material $Zn(CN)_2$ has been probed using atomic pair distribution function (PDF) analysis of high energy X-ray scattering data (100−400 K). The temperature dependence of the atomic separations extracted from the PDFs indicates an increase of the average transverse displacement of the cyanide bridge from the line connecting the Zn^{II} centers with increasing temperature. This allows the contraction of non-nearest-neighbor Zn···Zn′ and Zn···C/N distances despite the observed expansion of the individual direct Zn−C/N and C−N bonds. Thus, this analysis provides definitive structural confirmation that an increase in the average displacement of bridging atoms is the origin of the NTE behavior. The lattice parameters reveal a slight reduction in the NTE behavior at high temperature from a minimum coefficient of thermal expansion ($\alpha = dl/ldT$) of -19.8×10^{-6} K^{-1} below 180 K, which is attributed to interaction between the doubly interpenetrated frameworks that comprise the structure.

Introduction

Negative thermal expansion (NTE) behavior is an exotic material property with attractive potential applications,[1−3] most notably in moderating the predominantly positive thermal expansion (PTE) behavior of materials, particularly those in high precision applications where instability associated with temperature fluctuation often reduces performance. This behavior has been identified in a range of oxide-based materials containing strong single-atom bridges such as the AM_2O_8, AM_2O_7, $A_2M_3O_{12}$, and NASICON families. These include some tungstates (notably, ZrW_2O_8 and $Sc_2W_3O_{12}$),[4−7] molybdates (e.g., $ZrMo_2O_8$),[8] phosphates (e.g., $NbZr(PO_4)_3$ and ZrP_2O_7),[9,10] vanadates (e.g., ZrV_2O_7)[10] and many zeolites (e.g., ALPO-17 and chabazite).[11−13] More recently, NTE behavior has been recognized in molecular framework materials containing linear diatomic bridges such as the cyanide anion.[14−16] In both families of NTE materials, the increase in average transverse displacement of the bridging atoms, through thermal population of low energy transverse vibrational modes, with negligible expansion of the nearest-neighbor distances, is generally considered to induce a contraction of the next-nearest-neighbor separations and, accordingly, the lattice parameter.[5,15,17,18] The typical existence of rigid unit modes (RUMs)[19] in these systems, which model the possible lattice vibrations as the librational motion of corner sharing or bridged rigid polyhedra, is largely consistent with the proposed population of transverse vibrational modes.[15,20,21]

The direct experimental confirmation of the transverse vibrational mechanism for NTE has remained elusive and, indeed, this mechanism has been challenged in recent local structural studies which include variable temperature EXAFS studies on ZrW_2O_8[22] and in studies modeling the pair distribution function of the zeolite chabazite using a reverse Monte Carlo (RMC) approach.[23] The dynamic nature of these NTE materials

[†] University of Sydney.
[‡] Argonne National Laboratory.

(1) Evans, J. S. O. *J. Chem. Soc., Dalton Trans.* **1999**, 3317−3326.
(2) Sleight, A. W. *Annu. Rev. Mater. Sci.* **1998**, *28*, 29−43.
(3) Sleight, A. *Nature* **2003**, *425*, 674−676.
(4) Martinek, C.; Hummel, F. A. *J. Am. Ceram. Soc.* **1968**, *51*, 227−228.
(5) Evans, J. S. O.; David, W. I. F.; Sleight, A. W. *Acta Crystallogr., Sect. B: Struct. Sci.* **1999**, *55*, 333−340.
(6) Mary, T. A.; Evans, J. S. O.; Vogt, T.; Sleight, A. W. *Science (Washington, D. C.)* **1996**, *272*, 90−92.
(7) Evans, J. S. O.; Mary, T. A.; Sleight, A. W. *J. Solid State Chem.* **1997**, *133*, 580−583.
(8) Lind, C.; Wilkinson, A. P.; Hu, Z. B.; Short, S.; Jorgensen, J. D. *Chem. Mater.* **1998**, *10*, 2335−2337.
(9) Roy, R.; Agrawal, D. K.; McKinstry, H. A. *Annu. Rev. Mater. Sci.* **1989**, *19*, 59−81.
(10) Korthuis, V.; Khosrovani, N.; Sleight, A. W.; Roberts, N.; Dupree, R.; Warren, W. W. *Chem. Mater.* **1995**, *7*, 412−417.
(11) Lightfoot, P.; Woodcock, D. A.; Maple, M. J.; Villaescusa, L. A.; Wright, P. A. *J. Mater. Chem.* **2001**, *11*, 212−216.
(12) Attfield, M. P.; Sleight, A. W. *Chem. Mater.* **1998**, *10*, 2013−2019.
(13) Woodcock, D. A.; Lightfoot, P.; Villaescusa, L. A.; Diaz-Cabanas, M. J.; Camblor, M. A.; Engberg, D. *Chem. Mater.* **1999**, *11*, 2508−2514.
(14) Williams, D. J.; Partin, D. E.; Lincoln, F. J.; Kouvetakis, J.; O'Keeffe, M. *J. Solid State Chem.* **1997**, *134*, 164−169.
(15) Goodwin, A. L.; Kepert, C. J. *Phys. Rev. B* **2005**, *71*, 140301.
(16) Margadonna, S.; Prassides, K.; Fitch, A. N. *J. Am. Chem. Soc.* **2004**, *126*, 15390−15391.
(17) Barrera, G. D.; Bruno, J. A. O.; Barron, T. H. K.; Allan, N. L. *J. Phys.: Condens. Matter* **2005**, *17*, R217−R252.
(18) Tao, J. Z.; Sleight, A. W. *J. Solid State Chem.* **2003**, *173*, 442−448.
(19) Hammonds, K. D.; Dove, M. T.; Giddy, A. P.; Heine, V. *Am. Mineral.* **1994**, *79*, 1207−1209.
(20) Heine, V.; Welche, P. R. L.; Dove, M. T. *J. Am. Ceram. Soc.* **1999**, *82*, 1793−1803.
(21) Pryde, A. K. A.; Hammonds, K. D.; Dove, M. T.; Heine, V.; Gale, J. D.; Warren, M. C. *J. Phys.: Condens. Matter* **1996**, *8*, 10973−10982.
(22) Cao, D.; Bridges, F.; Kowach, G. R.; Ramirez, A. P. *Phys. Rev. B* **2003**, 68.

10.1021/ja055197f CCC: $30.25

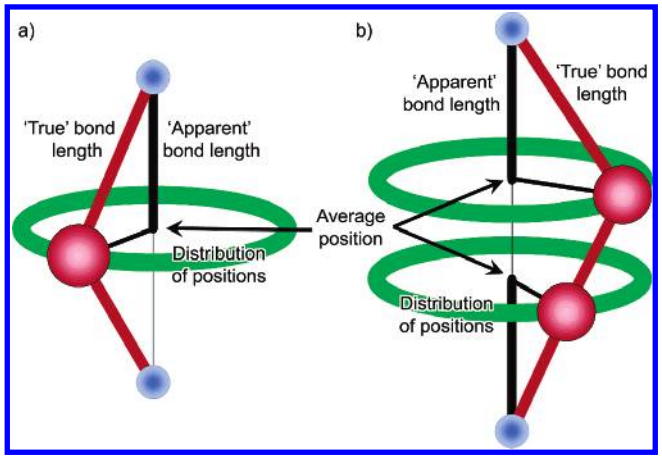

Figure 1. Representation of a single (a) and double-atom (b) bridged moiety in which a transverse vibration is excited. The 'apparent' bond length, which is inferred from the distance between the average positions of two atoms obtained from Bragg crystallographic analysis, and the 'true' bond length, which is the average distance between a pair of atoms, are indicated.

means that the instantaneous structure deviates considerably from the average structure measured by conventional crystallographic techniques reliant on analysis of Bragg intensities (Figure 1). Consequently, the application of Bragg analysis to NTE materials typically reveals an unphysical contraction, with increasing temperature, of the 'apparent' nearest-neighbor bond lengths inferred from the distance between the average positions of two atoms, and an elongation of the displacement parameters of the bridging atoms perpendicular to the bonding direction; features which are generally consistent with a transverse vibrational mechanism.[24−26]

In ZrW_2O_8, the oxide-based material exhibiting the most pronounced isotropic NTE, the contraction of the Zr−O−W linkages between the oxo-bridged ZrO_6 octahedra and WO_4 tetrahedra and, correspondingly, the lattice parameter, is accompanied by a contraction of the apparent Zr−O bond length as determined by Bragg techniques.[5] In the cyanide-bridged $Zn(CN)_2$ frameworks, which exhibit isotropic coefficients of thermal expansion (CTEs, $\alpha = dl/ldT$) up to more than double that of ZrW_2O_8, the increase in the average transverse vibrational amplitude of the cyanide bridge is suggested by the larger relative increase in the component of the C/N displacement parameter perpendicular to the Zn···Zn′ axis.[15] However, it is not clear that the harmonic approximation adequately describes any transverse vibrational motion and hence the magnitude of the displacement cannot be extracted reliably.

Total scattering approaches, which include atomic pair distribution function (PDF) analysis, have been applied successfully to probe the structure of systems containing dynamic disorder.[27,28] The PDF is a radial distribution function related to the probability of finding two atoms at a distance r (i.e., atom−atom correlations), including those which may deviate from the average long-range structure, providing insight into the instantaneous structure. As such, peaks in the PDF correspond to the average distance between pairs of atoms, that is, the 'true' bond lengths, which can be used to directly determine the magnitude of any displacement of bridging atoms from the bonding direction.

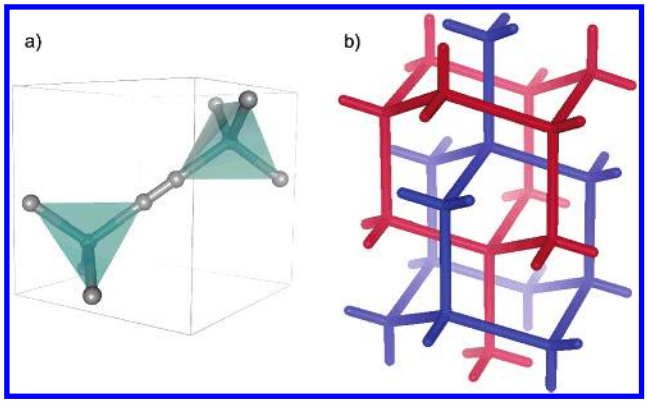

Figure 2. Representation of the cubic unit cell of the $Zn(CN)_2$-type framework indicating the tetrahedral $Zn(C/N)_4$ coordination (a) and an illustration of the network interpenetration (b). The Zn^{II} ions lie on special positions and the cyanide bridge is disordered (C/N−N/C) along the Zn···Zn′ axis of symmetry.

Here we report the direct observation of an increase in average transverse displacement with increasing temperature of the bridging atoms in $Zn(CN)_2$ through PDF analysis of variable temperature high energy X-ray scattering data. The advantage of this approach is that the structural information is extracted directly from the PDFs and, therefore, the interpretation of the data is not subject to artifacts that can arise from structural modeling[22,23] including from under-constrained (or over-constrained) models fitted through RMC methods.[29] The rich structural and compositional diversity of cyanide-bridged molecular framework materials is expected to yield a vastly expanded range of NTE materials with enhanced NTE properties arising from the additional flexibility associated with the double-atom bridge and, as such, the study of the mechanism underlying the NTE in the cyanide-bridged $Zn(CN)_2$ structure is of particular relevance.

The cubic $Zn(CN)_2$ structure ($Pn\bar{3}m$) consists of tetrahedral Zn^{II} centers bridged linearly by the cyanide anion to form a doubly interpenetrated expanded β−cristobalite-like framework (Figure 2).[14] In the Bragg analysis, the C/N bridging atoms are constrained to lie on the Zn···Zn′ 3-fold axis with the Zn^{II} centers in turn confined to special positions, highlighting the need for a total scattering approach to probe any transverse displacement. The observed increase in transverse displacement of the cyanide bridge corresponds to a contraction in non-nearest-neighbor distances which counteracts the observed expansion of the bond length for directly bonded atom pairs, confirming the population of transverse vibrational modes as the mechanism underlying the NTE behavior. This analysis also reveals the presence of longer range correlated lattice vibrations which can contribute to the NTE.

Experimental Section

Sample Preparation. Distilled water was carefully layered above aqueous solutions of $Zn(NO_3)_2{\cdot}6H_2O$ (0.22 g, 5 mL, 0.1 M) and K_2-$Zn(CN)_4$ (0.12 g, 5 mL, 0.1 M) contained within small glass vials

(23) Martinez-Inesta, M. M.; Lobo, R. F. *J. Phys. Chem. B* **2005**, *109*, 9389−9396.
(24) David, W. I. F.; Evans, J. S. O.; Sleight, A. W. *Europhys. Lett.* **1999**, *46*, 661−666.
(25) Li, J.; Yokochi, A.; Amos, T. G.; Sleight, A. W. *Chem. Mater.* **2002**, *14*, 2602−2606.
(26) Forster, P. M.; Sleight, A. W. *Int. J. Inorg. Mater.* **1999**, *1*, 123−127.
(27) Tucker, M. G.; Dove, M. T.; Keen, D. A. *J. Phys.: Condens. Matter* **2000**, *12*, L425−L430.
(28) Chupas, P. J.; Chaudhuri, S.; Hanson, J. C.; Qiu, X.; Lee, P. L.; Shastri, S. D.; Billinge, S. J. L.; Grey, C. P. *J. Am. Chem. Soc.* **2004**, *126*, 4756−4757.
(29) Tucker, M. G.; Dove, M. T.; Keen, D. A. *J. Appl. Crystallogr.* **2001**, *34*, 630−638.

and the vials placed inside a larger water filled glass beaker (total volume ca. 100 mL). Slow diffusion of the reagents resulted in crystalline samples of $Zn(CN)_2$ within 2−3 weeks. The samples were filtered, washed in water and ethanol, and dried in air.

Variable Temperature Powder X-ray Diffraction. The high energy X-rays (90.48 keV, $\lambda = 0.13702$ Å) available at the 11-ID-B beamline at the APS at Argonne National Laboratory were used in combination with a MAR-345 imaging plate (IP) detector to record diffraction patterns to high momentum transfers ($Q \approx 21$ Å^{-1}) for the sample housed in a polyimide capillary.[30] The sample was cooled to nominal temperature of 85 K using an Oxford Cryosystems Cryostream 700 and data were collected in 3 min exposures with continuous heating at a rate of 100 Khr^{-1} to a maximum temperature of 400 K. This corresponds to the collection of diffraction images at 7 K intervals. A temperature correction (see Supporting Information) was applied to the nominal temperature of the cryostream obtained from a calibration run with an Omega K-type thermocouple added at the sample position, such that the correct temperature range of the experiment was ca. 100−400 K. The sample-to-detector distance was increased for images used in Rietveld analysis to improve Q resolution. The raw images were processed using Fit-2D.[31,32] The sample-to-detector distance and tilt of the IP relative to the beam were refined using a LaB_6 calibrant.

PDF Analysis. The PDFs, $G(r) = 4\pi r[\rho(r) - \rho_o]$ where $\rho(r)$ and ρ_o are the instantaneous and average densities, were extracted using PDFgetX2,[33] subtracting the contributions from the sample environment and background to the measured diffraction intensities. Corrections for multiple scattering, X-ray polarization, sample absorption, and Compton scattering were then applied to obtain the structure function $S(Q)$. Direct Fourier transform of the reduced structure function $F(Q) = Q[S(Q) - 1]$ up to $Q_{max} \approx 21$ Å^{-1} gave $G(r)$, the pair distribution function. Distances of interest were extracted directly from the $G(r)$'s by direct fitting of a Gaussian function to the peaks at ∼2 Å ($d_{Zn-C/N}$) and ∼3.2 Å ($d_{Zn\cdots C/N}$) and the two peaks at ∼5 Å ($d_{Zn\cdots Zn}$ and $d_{Zn\cdots C/N'}$) within KUPLOT.[34] The distances reported are the average of duplicate variable temperature experiments. Although the termination ripples can influence the apparent peak positions, an effect which is most pronounced at low r, the rigorous treatment of this effect can be complicated by the fact that the low r-region also contains the most significant contribution from systematic errors in the data. Thus, improved fits are typically not obtained when termination ripples are considered, and a common approach is to fit only a Gaussian to the peak position.[35,36] To minimize any effect of the termination ripples, Fourier transforms were performed over a constant Q-range to ensure a consistent effect and to eliminate any influence on the observed change in the bond lengths and distances. Refinement of a model based on the Rietveld refined structure, against $G(r)$ and generation of partial PDFs were performed within PDFFIT.[37] A more complex starting configuration with the bridging atoms disordered over 6 positions displaced equidistant from the Zn···Zn′ axis was also refined.

Bragg Analysis. Structural analysis of the Bragg intensities within GSAS used the Rietveld method ($2\theta = 1.2-10.6°$; at 108 K $wR_p = 0.0287$, $R_p = 0.0222$; $R_{F^2} = 0.0487$; at 396 K $wR_p = 0.0275$, $R_p = 0.0211$; $R_{F^2} = 0.1062$).[38,39] Complete parameters from the Rietveld structural refinement are included in the Supporting Information. The lattice parameter, isotropic atomic displacement parameters, C/N position and peak shape parameters were refined independently at each temperature. The static disorder of the cyanide ligand was modeled with 50% C/N occupancy, with the C/N atoms constrained to have the same position and atomic displacement parameters. The CTEs, $\alpha = dl/ldT$, quoted for specific temperatures use the dl/dT fitted to 5 points in a ± 14 K range.

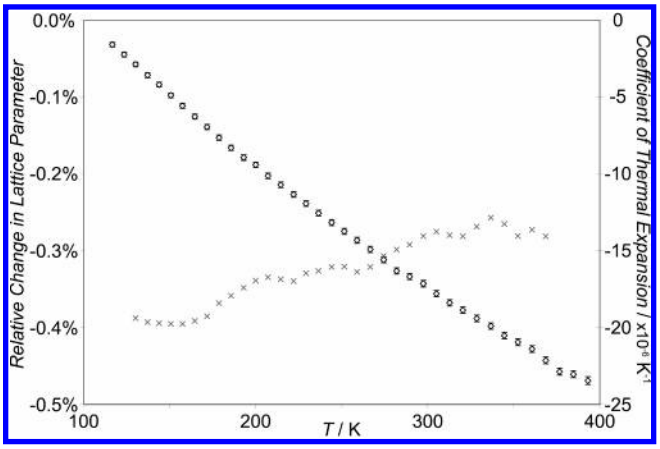

Figure 3. Temperature-dependent lattice parameters refined for $Zn(CN)_2$ relative to the lattice dimensions forecast at 100 K(◇) from Rietveld refinement of X-ray powder diffraction data (11-ID-B, APS). Error bars are given as ±1 esd. The corresponding isotropic coefficients of thermal expansion (×) are shown.

Results

Bragg Analysis. The refinement of the lattice parameters showed an isotropic contraction of the cubic lattice parameter in the temperature range 100−400 K (Figure 3).

While the NTE behavior appears approximately linear, with an average CTE of $-16.0(2) \times 10^{-6}$ K^{-1} (100−400 K), slight nonlinearities in the thermal expansion are evident. The CTE, which attains a minimum of -19.8×10^{-6} K^{-1} below 180 K, increases slightly at high temperature, approaching -14×10^{-6} K^{-1} at ca. 400 K.

Atomic Pair Distribution Function Analysis. The PDFs were obtained from the high energy X-ray scattering data by direct Fourier transform of the reduced structure functions, $F(Q)$, up to $Q \approx 21$ Å^{-1} (Figure 4a). The PDFs contain well-defined peaks to high r, as is consistent with the long range order requisite for Bragg crystallographic analysis (Figure 4b). The form of $G(r)$ evolves with increasing temperature, with general peak broadening and shifting of some peaks to lower r. The greatest changes, as a function of temperature, are evident at high r (> 6 Å). By contrast, the correlations that define the Zn^{II} coordination sphere (∼2 Å) do not change visibly.

Refinement of a model based on the crystallographic structure yielded a moderately good fit to the experimental PDF at 100 K ($R = 36.8\%$, Figure 5). Refinement of a more complex model in which the cyanide bridge is disordered over six equivalent positions displaced from the Zn···Zn′ axis yielded a slightly improved fit ($R = 34.9\%$). However, both models are unable to completely describe some of the long-range correlations with periodicities greater than a single unit cell, for example at $r \approx 12.5$, 17 Å. This is highly unusual for a crystalline system, for which the PDF fits usually improve at higher r, where the long-range structure approaches the average structure.[35] This indicates that there exists a greater extent of

(30) Chupas, P. J.; Qiu, X.; Hanson, J. C.; Lee, P. L.; Grey, C. P.; Billinge, S. J. L. *J. Appl. Crystallogr.* **2003**, *36*, 1342−1347.
(31) Hammersley, A. P.; Svensson, S. O.; Hanfland, M.; Fitch, A. N.; Häusermann, D. *High-Pressure Res.* **1996**, *14*, 235−248.
(32) Hammersley, A. P., *ESRF Internal Report* **1997**, ESRF97HA02T.
(33) Qiu, X.; Thompson, J. W.; Billinge, S. J. L. *J. Appl. Crystallogr.* **2004**, *37*, 678.
(34) Proffen, T.; Neder, R. B. *J. Appl. Crystallogr.* **1997**, *30*, 171−175.
(35) Qiu, X. Y.; Proffen, T.; Mitchell, J. F.; Billinge, S. J. L. *Phys. Rev. Lett.* **2005**, *94*, 177203.
(36) Peterson, P. F.; Bozin, E. S.; Proffen, T.; Billinge, S. J. L. *J. Appl. Crystallogr.* **2003**, *36*, 53−64.
(37) Proffen, T.; Billinge, S. J. L. *J. Appl. Crystallogr.* **1999**, *32*, 572−575.
(38) Toby, B. H. *J. Appl. Crystallogr.* **2001**, *34*, 210−213.
(39) Larson, A. C.; Von Dreele, R. B. *General Structure Analysis System (GSAS)* **2000**, Los Alamos National Laboratory Report, LAUR 86-748.

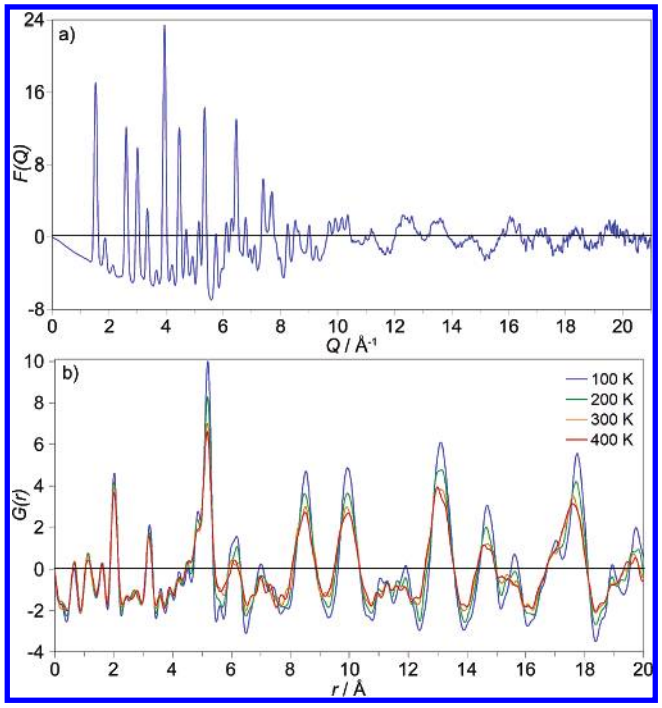

Figure 4. Reduced structure function, $F(Q) = Q[S(Q) - 1]$, at ca. 100 K (a) and the PDFs, $G(r)$, at representative temperatures (b) from high energy X-ray diffraction of $Zn(CN)_2$ (11-ID-B, APS).

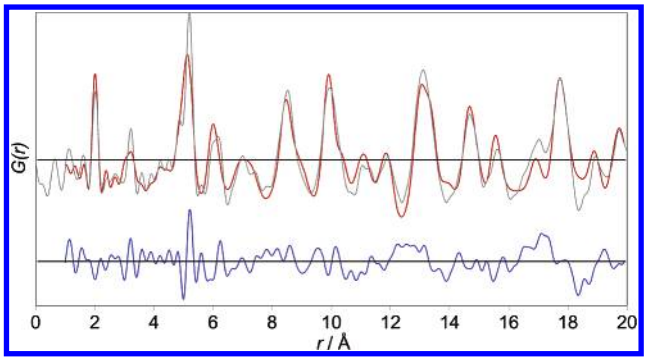

Figure 5. PDF generated for the crystallographic structural model (red) refined against the experimental PDF (gray). The residual (blue) is given below.

vibrational distortions than can be accounted for within a single unit cell. Thus, the PDF refinement suggests the existence of vibrational correlations with periodicities over several unit cells.

Reported analyses of vibrations involving in-phase atomic motion indicate that such vibrations are associated with a sharpening of correlations in the PDF.[40] Application of such sharpening for the first coordination shell, where there is obvious in-phase atomic motion, was attempted. However, comparison of the experimental and calculated PDF (Figure 5) shows that the peaks up to ca. 6 Å appear sharpened relative to the peaks at high r, suggesting correlation of longer range atomic motion. Analysis of this sharpening is beyond the scope of this paper and is currently being pursued in conjunction with refinement of a larger configuration model of multiple unit cells using a RMC modeling approach.[41]

(40) Jeong, I. K.; Proffen, T.; Mohiuddin-Jacobs, F.; Billinge, S. J. L. *J. Phys. Chem. A* **1999**, *103*, 921−924.
(41) Nield, V.; Keen, D. A. *Diffuse Neutron Scattering from Crystalline Materials*; Oxford/Clarendon Press: New York, 2001.

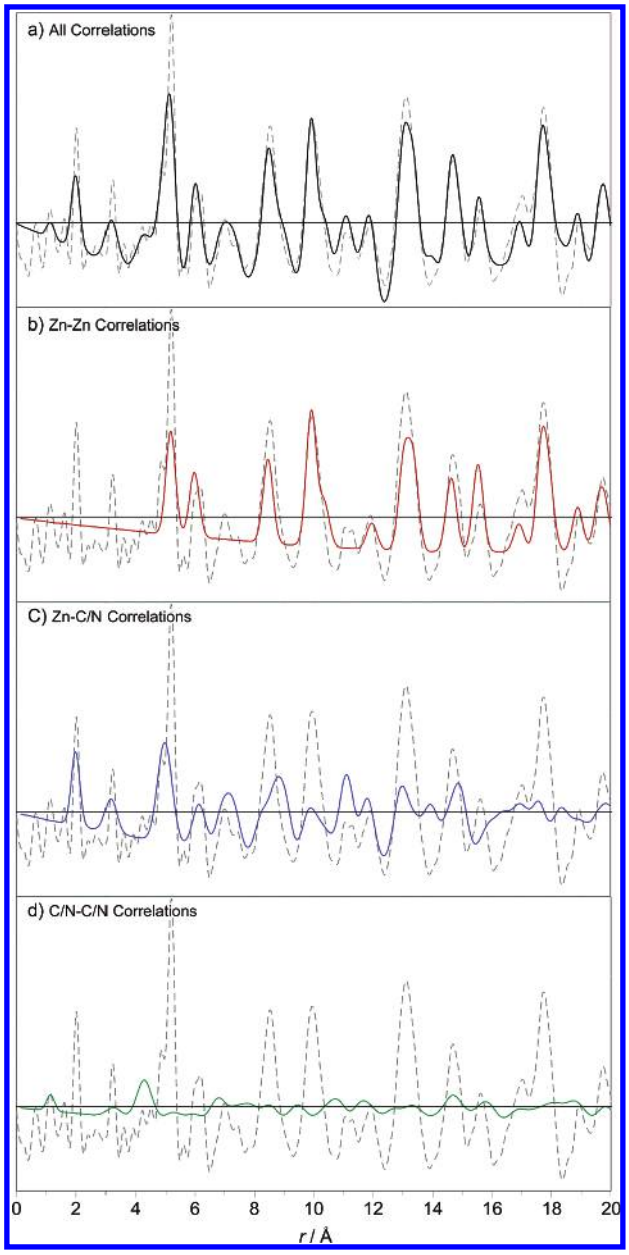

Figure 6. Calculated total PDF (a) and the partial PDFs corresponding to Zn−Zn (b), Zn−C/N (c), and C/N−C/N (d) correlations, calculated for the structural model based on the crystalline Bragg starting configuration for $Zn(CN)_2$ at 100 K. No peak sharpening, arising from correlated atomic motion, has been included. The experimental PDF (gray dashed line) has been overlaid for comparison.

The peaks in the PDFs correspond principally to Zn−Zn and Zn−C/N correlations (Figure 6). The low intensity correlations between the carbon and nitrogen atoms, which have low scattering power relative to zinc, are of the same order as the termination ripples arising from the direct Fourier transform of $F(Q)$, which are most pronounced in the low r region, and, as such, cannot be extracted accurately.

The individual peaks below $r \approx 6$ Å, corresponding to Zn−Zn and Zn−C/N atomic correlations, were identified and fit with a Gaussian function to extract accurate peak positions, that is, bond lengths and distances, as a function of temperature (Figure 7).[32]

The bond lengths and distances from the Bragg and PDF analyses, and their corresponding temperature dependence, show

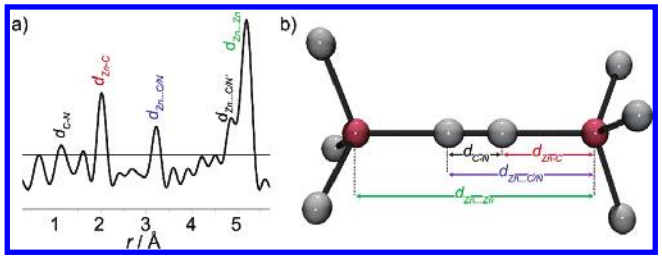

Figure 7. Peaks in the PDF below $r \approx 6$ Å (a) relate to the shortest local atomic correlations corresponding to the direct C−N and Zn−C/N distances, non-nearest-neighbor Zn···C/N and Zn···Zn′ intra-framework distances and Zn···C/N′ inter-framework distance.

Table 1. Selected Distances and the Corresponding CTEs from Bragg and PDF Analysis

	Bragg analysis			PDF analysis		
	d(100K)/ Å	*d*(400K)/ Å	CTE/ × $10^{-6}K^{-1}$	*d*(100K)/ Å	*d*(400K)/ Å	CTE/ × $10^{-6}K^{-1}$
C−N	1.200	1.194	−19(5)			
Zn−C/N	1.986	1.977	−15.1(16)	2.015	2.021	+10.2(10)
Zn···C/N	3.186	3.171	−16.4(8)	3.209	3.203	−6.4(10)
Zn···C/N′$_{\text{other net}}$	4.883	4.860	−15.8(2)	4.871	4.837	−23(4)
Zn···Zn′	5.172	5.147	−15.9(2)	5.191	5.172	−12.42(12)

significant differences (Table 1). The apparent bond lengths and distances inferred from the average atomic positions (Bragg) are contracted relative to the 'true' (PDF) distances, a feature that is consistent with a difference in the average and instantaneous structures. The Zn−C/N bond length from the Bragg analysis appears to contract with increasing temperature (Figure 8), contradicting known behavior for directly bonded atoms for which thermal expansion occurs due to the inherent anharmonicity of the interatomic potential. In contrast, the true Zn−C/N bond length from the PDF analysis expands with increasing temperature. Again, this feature is consistent with an increase in the deviation of the average and instantaneous structures at higher temperatures.

The average displacement (D) of the C/N bridging atoms from to line connecting the Zn^{II} centers can be calculated directly from the PDF results according to the geometric relation

$$D = \sqrt{(d_{\text{Zn-C/N}})^2 - \left(\frac{(d_{\text{Zn-C/N}})^2 + (d_{\text{Zn}\cdots\text{Zn}})^2 - (d_{\text{Zn}\cdots\text{C/N}})^2}{2d_{\text{Zn}\cdots\text{Zn}}}\right)^2}$$

where $d_{\text{Zn-C/N}}$, $d_{\text{Zn}\cdots\text{C/N}}$ and $d_{\text{Zn}\cdots\text{Zn}'}$ are the Zn−C/N, Zn···C/N, and Zn···Zn′ distances extracted from the PDF (Figure 9).

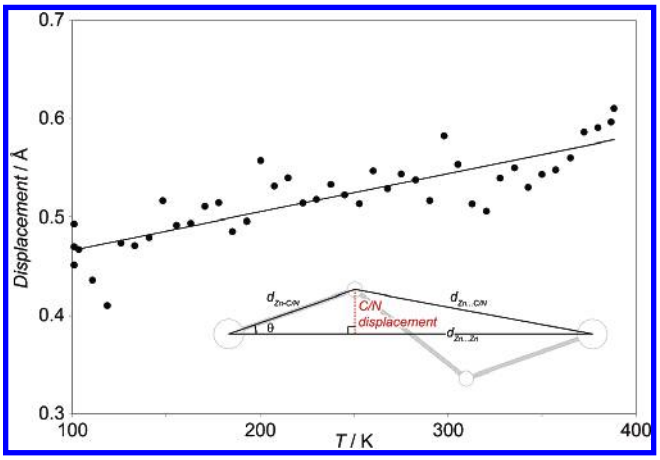

Figure 9. Average displacement of the C/N bridging atoms from the line connecting the Zn^{II} centers. The straight line is the linear least-squares fit to the data.

The average transverse displacement increases with increasing temperature by 0.04 Å per 100 K from 0.46 Å at 100 K to 0.58 Å at 400 K.

The range of the direct C−N bond length can also be derived from the PDF distances based on the two extremes of the displacement modes with the two bridging atoms to the same side of the Zn···Zn′ axis and to opposite sides of the Zn···Zn′ axis (Figure 10). These both show the correct PTE behavior.

Discussion

The PDF analysis provides direct evidence of the increase in the average displacement of the C/N bridging atoms from the Zn···Zn′ direction at higher temperatures. This induces the contraction of the non-nearest-neighbor Zn···C/N and Zn···Zn′ distances, despite the observed expansion of the nearest-neighbor Zn−C/N and C−N bond lengths which is associated with the inherent anharmonicity of the interatomic potential for directly bonded atom pairs. The Bragg analysis shows the opposite, unphysical trend for the apparent direct Zn−C/N and C−N bond lengths, confirming the necessity of a total scattering approach to accurately determine the temperature dependence of atomic correlations in the dynamic structure. A similar discrepancy in the high-temperature bond lengths from Bragg and total scattering approaches has been demonstrated by Keen and coworkers for the related β-cristobalite (SiO_2) structure.[27] Thus,

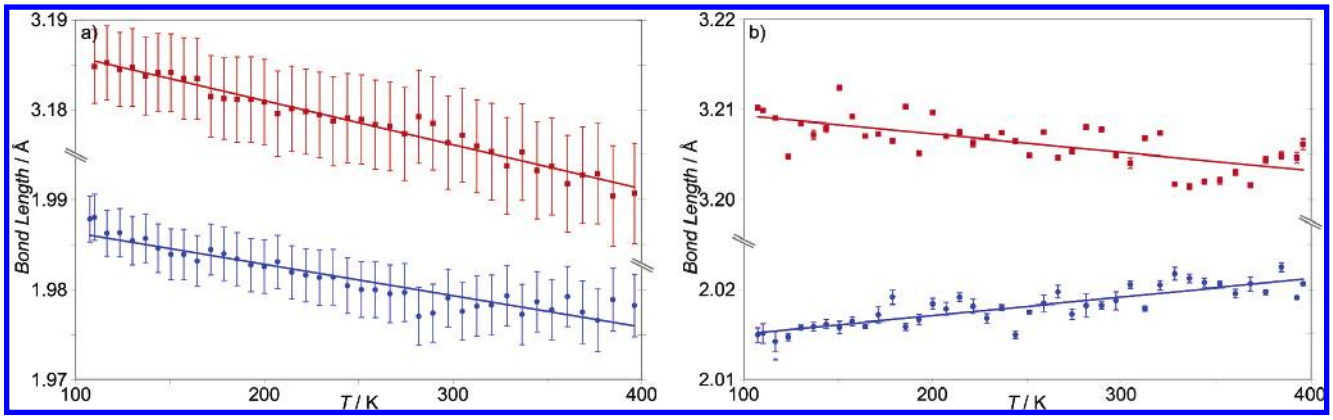

Figure 8. Temperature-dependent Zn−C/N bond length (●) and next-nearest-neighbor Zn···C/N distance (■), as inferred from the average atomic positions from the Bragg analysis (a) and as extracted from the PDFs (b). Error bars are given as ±1 esd.[42] The straight lines are the least-squares fit to the data.

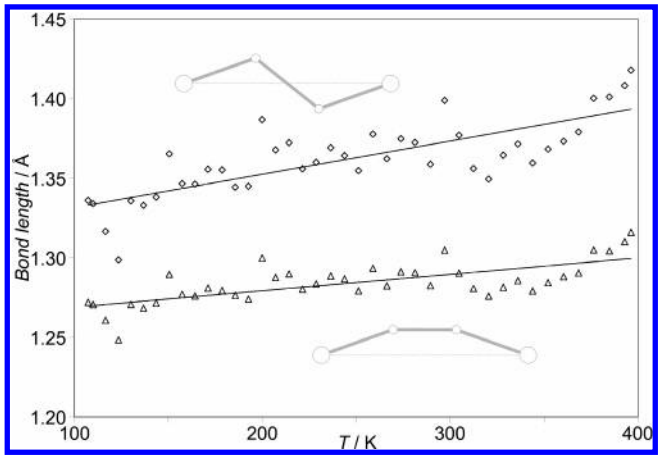

Figure 10. Expansion of the direct C−N bond lengths calculated from the PDF distances assuming displacement of bridging atoms in opposite (◇) and identical (△) directions. The straight lines are linear least-squares fits to the data.

the PDF analysis confirms the increase in the transverse vibrational motion of the bridging atoms as the origin of the observed NTE behavior.

The PDF analysis indicates a PTE contribution from the individual bond lengths that to some extent counteracts the NTE influence of the transverse vibrations of the cyanide bridge. Although the generally stated mechanism for NTE in such systems assumes that bond length PTE effects are minor, the present analysis clearly indicates a large PTE behavior for the Zn−C/N bond length with a CTE of $+10.2(10) \times 10^{-6}$ K^{-1}, considerably larger than the Si−O bond expansion coefficient ($+2.2 \times 10^{-6}$ K^{-1})[27] such as in β-cristobalite and greater in magnitude than the bulk NTE in ZrW_2O_8 (-9.1×10^{-6} K^{-1}).[5] Previous analyses of the atomic displacement parameters, which assume harmonic motion, were in apparent agreement with thermal expansion data,[15] however, such analyses assume negligible expansion of the individual bond lengths,[43] an effect which the present study demonstrates to be more significant that previously postulated. It is noteworthy that the more significant NTE contribution from the transverse vibrations of the cyanide bridge in this highly flexible material[15] is sufficient to produce a large overall NTE property.

The PDF analysis shows a significantly less rapid contraction of the intra-framework Zn···Zn′ distance than for the Bragg distance or lattice parameter. This suggests a contribution from lattice vibrations with displacement of the Zn^{II} ions from the special positions to which they were confined in the Bragg analysis, such that the true Zn···Zn′ distance is greater than the Bragg distance. Correlated vibrations moving atoms off special positions are also evident in other types of dynamic structures, including perovskites. For example, in the high-temperature cubic form of AlF_3, which exhibits the ReO_3 structure, transverse vibrational motion has been identified using the PDF method[28] (although for AlF_3 this effect is not sufficient to counteract the significant PTE of the individual Al−F bonds). In the dynamic structure, the rigid AlF_6 octahedra are involved in correlated motions around their 3-fold symmetry axis in which the Al atoms move off the special positions. The same effect is expected to be true in $Zn(CN)_2$ with displacement of the Zn^{II} ions from the special positions.

The observed reduction in the NTE behavior at higher temperatures may be due to dampening of high amplitude vibrations, such as through steric interaction of the interpenetrated frameworks. The closest inter-framework interaction between the interpenetrated frameworks is between the midpoints of the cyanide bridges, an interaction that will be influenced significantly by the amplitude of the transverse displacement of these bridges. Disregarding any correlation in this transverse displacement between frameworks, the PDF results indicate that the average distance between bridging atoms if displaced directly toward each other decreases from 3.29 Å at 100 K to 3.04 Å at 400 K, thus bringing the inter-framework contacts within the van der Waals radii. The unfavorable nature of such an interaction suggests that a degree of correlation may exist between the vibrational modes in the interpenetrated frameworks to avoid this steric interaction. Thus, increasing inter-framework correlations may be responsible for the subtle reduction in the NTE at higher temperatures (>180 K). The $Zn(CN)_2$ family are the only NTE materials yet reported with an interpenetrated structure and hence this effect has not been observed previously, although the thermal expansion of unrelated guests is known to influence the NTE in porous zeolites.[44]

Both the correlated vibrations of the Zn^{II} centers and the interpenetrated framework are associated with periodicities beyond a single unit cell and may therefore be responsible for the poor fit of the crystallographic model to the PDF at high *r*.

Conclusion

The application of PDF methods to probe the structure of the NTE material $Zn(CN)_2$ provides unique insights into the dynamic structure that cannot be obtained with traditional Bragg crystallography. The PDF analysis provides definitive evidence of the increasing average transverse displacement of the cyanide bridge with increasing temperature, confirming the population of transverse vibrational modes of the bridging atoms as the mechanism underlying the NTE behavior. The data further show that this effect is sufficient to counteract the PTE contribution from the significant thermal expansion of the individual Zn−C/N bond lengths. Modeling of the PDF suggests vibrational correlations that extend beyond a single unit cell, such as involving the correlated displacements of the Zn^{II} centers from the special positions and interaction between the pairs of interpenetrated frameworks. We propose that the latter may cause a slight reduction in the NTE at high temperature.

Application of a PDF approach can be readily envisioned to study thermal expansion in a variety of materials including other cyanide-bridged frameworks such as the Prussian blue analogues,[16] oxide-based NTE materials, and systems that display anomalous thermal expansion due to other mechanisms.[45−47]

Acknowledgment. This work was supported by the Australian Synchrotron Research Program, which is funded by the Com-

(42) The esd's for the bond length extracted from the PDF are taken as the esd for the Gaussian fit to the peak. Systematic errors in the measurement of $S(Q)$ tend to occur as long wavelength modulations in $S(Q)$. Thus, the systematic errors in the PDF are most pronounced at low *r*, where actual error in the values contains a component associated with the systematic errors. See Toby, B. H.; Billinge, S. J. L. *Acta Crystallogr., Sect. A: Fundam. Crystallogr.* **2004**, *60*, 315−317.

(43) Busing, W. R.; Levy, H. A. *Acta Crystallogr.* **1964**, *17*, 142−146.
(44) Jardim, P. M.; Marinkovic, B. A.; Saavedra, A.; Lau, L. Y.; Baehtz, C.; Rizzo, F. *Micropor. Mesopor. Mater.* **2004**, *76*, 23−28.
(45) Salvador, J. R.; Guo, F.; Hogan, T.; Kanatzidis, M. G. *Nature* **2003**, *425*, 702−705.
(46) Jayarama, A.; Bucher, E.; Dernier, P. D.; Longinot, L. *Phys. Rev. Lett.* **1973**, *31*, 700−703.
(47) Arvanitidis, J.; Papagelis, K.; Margadonna, S.; Prassides, K.; Fitch, A. N. *Nature* **2003**, *425*, 599−602.

monwealth of Australia under the Major National Research Facilities. Work performed at the A.P.S. was supported by the U.S. D.o.E., Office of Science, Basic Energy Sciences, under Contract No. W-31-109-Eng-38. C.J.K. thanks A. L. Goodwin for valuable discussions. We thank C. Kurtz, G. Jennings, and N. Leyarovska for experimental support.

Supporting Information Available: Details of PDF and Bragg analysis (PDF). This material is available free of charge via the Internet at http://pubs.acs.org.

JA055197F